Mitigation of Rayleigh backscattering in 10-Gb/s downstream and 2.5-Gb/s upstream DWDM 100-km long-reach PONs

C. W. Chow[1,*] and C. H. Yeh[2,3]

[1]*Department of Photonics and Institute of Electro-Optical Engineering, National Chiao Tung University, Hsinchu 30010, Taiwan*

[2]*Information and Communications Research Laboratories, Industrial Technology Research Institute (ITRI), Hsinchu 31040, Taiwan*

[3]*depew@itri.org.tw*

[*]*cwchow@faculty.nctu.edu.tw*

Abstract: Long-reach passive optical network (LR-PON) is considered as a promising technology towards higher capacity and extended coverage optical system. We propose and demonstrate a LR-PON with the capability of Rayleigh backscattering (RB) noise mitigation. By using the upstream signal wavelength-transition generated by a dual-parallel Mach-Zehnder modulator (DP-MZM) based colorless optical networking unit (ONU), the spectral overlap among the upstream signal and the RB noises can be minimized. Hence, due to the achievement of effective RB mitigation, a 100 km LR-PON with a high split-ratio of 512 is demonstrated using 10 Gb/s non-return-to-zero (NRZ) downstream and 2.5 Gb/s NRZ upstream signals. Detail analysis of the wavelength-transition generation is presented.

OCIS codes: (060.0060) Fiber optics and optical communications; (060.2360) Fiber optics links and subsystems; (350, 4010) Microwaves.

References and links

1. I. Van de Voorde, C. M. Martin, J. Vandewege, and X. Z. Oiu, "The SuperPON demonstrator: an exploration of possible evolution paths for optical access networks," IEEE Commun. Mag. **38**(2), 74–82 (2000).
2. D. B. Payne, and R. P. Davey, "The Future of fiber access systems," BT Technol. J. **20**(4), 104–114 (2002).
3. G. Talli, C. W. Chow, E. K. MacHale, and P. D. Townsend, "Rayleigh noise mitigation in long-reach hybrid DWDM-TDM PONs," J. Opt. Netw. **6**, 765–776 (2007).
4. I. T. Monroy, F. Öhman, K. Yvind, R. Kjaer, C. Peucheret, A. M. J. Koonen, and P. Jeppesen, "85 km long reach PON system using a reflective SOA-EA modulator and distributed Raman fiber amplification," Proc. LEOS Annual Meeting, Paper WEE4 (2006).
5. C. W. Chow, C. H. Yeh, C. H. Wang, F. Y. Shih, C. L. Pan, and S. Chi, "WDM extended reach passive optical networks using OFDM-QAM," Opt. Express **16**(16), 12096–12101 (2008).
6. C. H. Wang, C. W. Chow, C. H. Yeh, C. L. Wu, S. Chi, and C. Lin, "Rayleigh noise mitigation using single sideband modulation generated by a dual-parallel MZM for carrier distributed PON," IEEE Photon. Technol. Lett. **22**(11), 820–822 (2010).
7. C. W. Chow, and C. H. Yeh, "Long-reach WDM PONs," Proc. IEEE Photonics Society Annual Meeting, Invited Talk WA1 (2010).
8. C. W. Chow, G. Talli, and P. D. Townsend, "Rayleigh noise reduction in 10-Gb/s DWDM-PONs by wavelength detuning and phase-modulation-induced spectral broadening," IEEE Photon. Technol. Lett. **19**(6), 423–425 (2007).
9. Z. Li, Y. Dong, Y. Wang, and C. Lu, "A novel PSK—Manchester modulation format in 10-Gb/s passive optical network system with high tolerance to beat interference noise," IEEE Photon. Technol. Lett. **17**(5), 1118–1120 (2005).
10. M. T. Abuelma'atti, "Large signal analysis of the Mach-Zehnder modulator with variable bias," Proc. Natl. Sci. Counc. ROC(A) **25**, 254–258 (2001).
11. O. Leclerc, P. Brindel, D. Rouvillain, E. Pincemin, B. Dany, E. Desurvire, C. Duchet, E. Boucherez, and S. Bouchoule, "40 Gbit/s polarization-insensitive and wavelength-independent InP Mach-Zehnder modulator for all-optical regeneration," Electron. Lett. **35**(9), 730–732 (1999).

#140988 - $15.00 USD Received 12 Jan 2011; revised 7 Feb 2011; accepted 7 Feb 2011; published 1 Mar 2011

1. Introduction

Fiber-to-the-home (FTTH) is being deployed all over the world and passive optical network (PON) is a promising FTTH access network architecture connecting many end-users to the central office (CO) cost-effectively. For further cost reduction, an alternative network architecture, dense-wavelength-division-multiplexing (DWDM) long-reach PON (LR-PON) [1–7], has been proposed and demonstrated to extend the PON coverage from 20 km to 100 km. Optical amplifiers are usually included to support the extended reach and the high split-ratio. Using optical carrier-distribution and wavelength independent (colorless) optical networking units (ONUs) can simplify the administration of the wavelength assignment to different ONUs and solve the inventory issue of using different wavelength-specific lasers in the ONU and CO. However, these carrier-distributed LR-PONs suffer from Rayleigh backscattering (RB) interferometric beat noises at the upstream signal. RB mitigation using phase-modulation-induced spectral broadening with offset filtering [8] and using phase shift keying (PSK) - Manchester formats [9] are proposed, but the scheme removes more than half of the upstream signal power and requires complicated coding and decoding respectively.

In this work, we propose and demonstrate a LR-PON capable of RB noises mitigation. By using the upstream signal wavelength-transition generated by a commercially available dual-parallel Mach-Zehnder modulator (DP-MZM) based colorless ONU, the spectral overlap among the upstream signal and the RB noises can be minimized. Hence, owing to the effective mitigation of the RB, a 100 km LR-PON with a high split-ratio of 512 is achieved. The upstream signal is in NRZ format; hence conventional direct-detection can still be used. Detail analysis of the wavelength-transition generation is presented. Both dominant RB noise sources, named the carrier-generated RB (Carrier-RB) and the signal-generated RB (Signal-RB) are significantly mitigated.

2. RB noise sources in the carrier-distributed LR-PON

As shown in Fig. 1(a), there are two main RB noise sources in the carrier-distributed LR-PON: Carrier-RB is generated by the backscattering of the continuous-wave (CW) optical carrier delivered to the ONU; and Signal-RB is generated by backscattering of the upstream data signal, which will be modulated again at the ONU before sending to the CO. For conventional non-return-to-zero (NRZ) signal as shown in Fig. 1(a), high RB noises occur due to a high spectral overlap among the upstream signal the both Carrier-RB and Signal-RB. Figure 1(b) shows the proposed RB mitigation LR-PON using wavelength-transition. By transiting the wavelength away from the distributed CW carrier, Carrier-RB can be mitigated. The upstream signal will be modulated by the ONU and transit again away from its original wavelength; hence Signal-RB can be mitigated, as shown in Fig. 1(b).

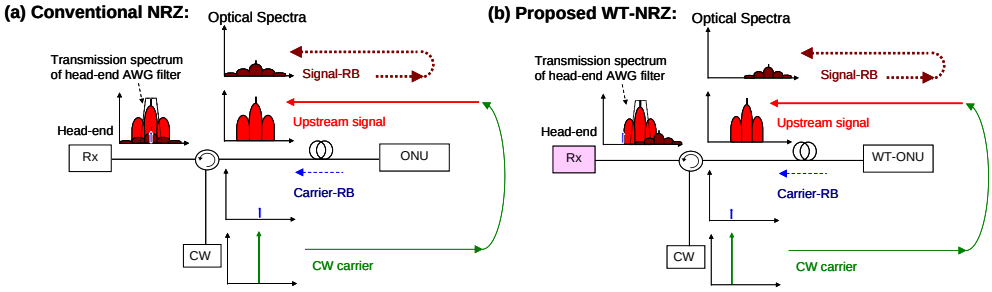

Fig. 1. Schematics of carrier-distributed PONs using (a) conventional NRZ and proposed WT-NRZ signal.

3. Principle of wavelength-translation generated by a DP-MZM

In this section, we will show the idea of wavelength-transition by a DP-MZM using mathematical analysis. Figure 2 shows the schematic architecture of the DP-MZM and the

#140988 - $15.00 USD Received 12 Jan 2011; revised 7 Feb 2011; accepted 7 Feb 2011; published 1 Mar 2011

insets show different optical frequency components generated at different locations of the DP-MZM. The blue and blown arrows represent the even and odd harmonics of the signals respectively. The directions of the arrows show the positive or negative signs of the signals. The DP-MZM was commercially available with a modulation bandwidth of 12 GHz. The baseband 2.5 Gb/s NRZ data was first mixed with an electrical sinusoidal signal at frequency f_s (10 GHz) via a radio-frequency (RF) mixer. It was then split into two paths by a 90° hybrid power-splitter and drove the DP-MZM in-phase and quadrature-phase at the upper MZM_1 and the lower MZM_2 respectively. We can consider each MZM consists of 2 phase modulators arranged in a MZ structure. The output E-field for the upper arm in the MZM_1 is shown in Eq. (1).

$$\begin{aligned} E_{MZM1-upper}(t) &= \mathrm{Re}\left\{\frac{1}{\sqrt{2}}E_0 e^{j(\omega_0 t+\Delta\varphi)}\right\} = \frac{1}{\sqrt{2}}E_0\cos(\omega_0 t+\Delta\varphi) \\ &= \frac{1}{\sqrt{2}}E_0\left\{\cos\omega_0 t\cos\Delta\varphi - \sin\omega_0 t\sin\Delta\varphi\right\} \end{aligned} \tag{1}$$

where ω_0 and $\Delta\varphi$ are angular frequency and phase difference induced by the applied voltage to the phase modulator respectively. In order to simplify the analysis, we assume the applied electrical signal is sinusoidal with amplitude and frequency of m and ω_{RF} respectively. Hence, the voltage induced phase change to the upper phase modulator in MZM_1 is shown in Eq. (2).

$$\Delta\varphi(t) = m\cos(\omega_{RF}t) \tag{2}$$

By substituting Eq. (2) into Eq. (1), we have Eq. (3).

$$\begin{aligned} E_{MZM1-upper}(t) &= \frac{1}{\sqrt{2}}E_0\left\{\begin{matrix}\cos\omega_0 t\cos\left[m\cos\left(\omega_{RF}t\right)\right] \\ -\sin\omega_0 t\sin\left[m\cos\left(\omega_{RF}t\right)\right]\end{matrix}\right\} \\ &= \frac{1}{\sqrt{2}}E_0\left\{\cos\omega_0 t\left[\begin{matrix}J_0(m) \\ +2\sum_{n=1}^{\infty}(-1)^n J_{2n}(m)\cos(2n\omega_{RF}t)\end{matrix}\right]\right. \\ &\quad \left.-\sin\omega_0 t\left[2\sum_{n=1}^{\infty}(-1)^n J_{2n-1}(m)\cos\left[\left(2n-1\right)\omega_{RF}t\right]\right]\right\} \end{aligned} \tag{3}$$

where $J_n(m)$ is the Bessel function. By using the Bessel function identifies in [10], we then expand Eq. (3) and neglect the higher order ($n \geq 4$) terms since their values are small. The output E-field becomes Eq. (4).

$$\begin{aligned} E_{MZM1-upper}(t) &\cong \frac{1}{\sqrt{2}}E_0\left\{\cos\omega_0 t\left[J_0(m) - 2J_2(m)\cos(2\omega_{RF}t)\right]\right. \\ &\quad \left.-\sin\omega_0 t\left[-2J_1(m)\cos(\omega_{RF}t) + 2J_3(m)\cos(3\omega_{RF}t)\right]\right\} \\ &= \frac{1}{\sqrt{2}}E_0\left\{J_0(m)\cos\omega_0 t - J_2(m)\left[\begin{matrix}\cos(\omega_0 t+2\omega_{RF}t) \\ +\cos(\omega_0 t-2\omega_{RF}t)\end{matrix}\right]\right. \\ &\quad + J_1(m)\left[\sin(\omega_0 t+\omega_{RF}t)+\sin(\omega_0 t-\omega_{RF}t)\right] \\ &\quad \left.-J_3(m)\left[\sin(\omega_0 t+3\omega_{RF}t)+\sin(\omega_0 t-3\omega_{RF}t)\right]\right\} \end{aligned} \tag{4}$$

This can be illustrated in the schematic optical spectra shown in Fig. 2(a). Since the E-field applied to the lower phase modulator in the MZM_1 is opposite to that of the upper phase modulator, the phase shift is negative as shown in Eq. (5).

#140988 - $15.00 USD Received 12 Jan 2011; revised 7 Feb 2011; accepted 7 Feb 2011; published 1 Mar 2011

$$\Delta\varphi(t) = -m\cos(\omega_{RF}t) \tag{5}$$

By substituting Eq. (5) into Eq. (1), we have Eq. (6).

$$\begin{aligned} E_{MZM1-lower}(t) &= \frac{1}{\sqrt{2}}E_0\begin{Bmatrix}\cos\omega_0 t\cos\left[-m\cos(\omega_{RF}t)\right]\\ -\sin\omega_0 t\sin\left[-m\cos(\omega_{RF}t)\right]\end{Bmatrix}\\ &= \frac{1}{\sqrt{2}}E_0\begin{Bmatrix}\cos\omega_0 t\cos\left[m\cos(\omega_{RF}t)\right]\\ +\sin\omega_0 t\sin\left[m\cos(\omega_{RF}t)\right]\end{Bmatrix}\\ &= \frac{1}{\sqrt{2}}E_0\left\{\cos\omega_0 t\left[J_0(m)+2\sum_{n=1}^{\infty}(-1)^n J_{2n}(m)\cos\left(2n\omega_{RF}t\right)\right]\right.\\ &\quad\left.+\sin\omega_0 t\left[2\sum_{n=1}^{\infty}(-1)^n J_{2n-1}(m)\cos\left[\left(2n-1\right)\left(\omega_{RF}t\right)\right]\right]\right\} \end{aligned} \tag{6}$$

Similarly, higher order ($n \geq 4$) terms can be neglected.

$$\begin{aligned} E_{MZM1-lower}(t) &\cong \frac{1}{\sqrt{2}}E_0\left\{\cos\omega_0 t\begin{bmatrix}J_0(m)\\ -2J_2(m)\cos(2\omega_{RF}t)\end{bmatrix}\right.\\ &\quad\left.+\sin\omega_0 t\left[-2J_1(m)\cos(\omega_{RF}t)+2J_3(m)\cos(3\omega_{RF}t)\right]\right\}\\ &= \frac{1}{\sqrt{2}}E_0\left\{J_0(m)\cos\omega_0 t - J_2(m)\begin{bmatrix}\cos(\omega_0 t+2\omega_{RF}t)\\ +\cos(\omega_0 t-2\omega_{RF}t)\end{bmatrix}\right.\\ &\quad -J_1(m)\left[\sin(\omega_0 t+\omega_{RF}t)+\sin(\omega_0 t-\omega_{RF}t)\right]\\ &\quad\left.+J_3(m)\left[\sin(\omega_0 t+3\omega_{RF}t)+\sin(\omega_0 t-3\omega_{RF}t)\right]\right\} \end{aligned} \tag{7}$$

This can be illustrated in the schematic optical spectra shown in Fig. 2(b). When the dc bias to the MZM_1 is V_π, the Bessel terms in Eq. (7) will rotate by π, as shown in Fig. 2(c). Finally, Fig. 2(d) presents the combined output of MZM_1.

For the MZM_2, since the applied electrical signal is π/2 phase-shifted by the 90° power splitter, the voltage-induced phase change to the upper phase modulator is shown in Eq. (8).

$$\Delta\varphi(t) = m\cos\left(\omega_{RF}t+\frac{\pi}{2}\right) = -m\sin\left(\omega_{RF}t\right) \tag{8}$$

By performing the similar mathematical analysis as above, the E-field at the upper phase modulator of MZM_2 (Fig. 2(e)) is shown in Eq. (9).

$$\begin{aligned} E_{MZM2-upper}(t) &\cong \frac{1}{\sqrt{2}}E_0\left\{J_0(m)\cos\omega_0 t - J_2(m)\begin{bmatrix}\cos\left(\omega_0 t+2\omega_{RF}t\right)\\ +\cos\left(\omega_0 t-2\omega_{RF}t\right)\end{bmatrix}\right.\\ &\quad -J_1(m)\left[\cos\left(\omega_0 t+\omega_{RF}t\right)-\cos\left(\omega_0 t-\omega_{RF}t\right)\right]\\ &\quad\left.-J_3(m)\left[\cos\left(\omega_0 t+3\omega_{RF}t\right)-\cos\left(\omega_0 t-3\omega_{RF}t\right)\right]\right\} \end{aligned} \tag{9}$$

Similarly, since the E-field applied to the lower phase modulator in the MZM_2 is opposite to that of its upper phase modulator, the phase shift is shown in Eq. (10).

$$\Delta\varphi(t) = -m\cos\left(\omega_{RF}t+\frac{\pi}{2}\right) = m\sin\left(\omega_{RF}t\right) \tag{10}$$

By substituting Eq. (10) into Eq. (1), we have Eq. (11).

#140988 - $15.00 USD Received 12 Jan 2011; revised 7 Feb 2011; accepted 7 Feb 2011; published 1 Mar 2011

$$E_{MZM\,2-lower}(t) \cong \frac{1}{\sqrt{2}} E_0 \left\{ J_0(m)\cos\omega_0 t + J_2(m)\begin{bmatrix}\cos(\omega_0 t + 2\omega_{RF} t)\\ +\cos(\omega_0 t - 2\omega_{RF} t)\end{bmatrix} \right.$$
$$+ J_1(m)\left[\cos(\omega_0 t + \omega_{RF} t) - \cos(\omega_0 t - \omega_{RF} t)\right] \qquad (11)$$
$$\left. + J3(m)\left[\cos(\omega_0 t + 3\omega_{RF} t) - \cos(\omega_0 t - 3\omega_{RF} t)\right] \right.$$

This can be illustrated in the schematic optical spectra shown in Fig. 2(f). When the dc bias to the MZM_2 is V_π, the Bessel terms in Eq. (11) will rotate by π, as shown in Fig. 2(g). Figure 2(h) shows the combined output of MZM_2.

Finally, when the dc bias to the MZM_3 of the DP-MZM is $V_\pi/2$, the Bessel terms shown in Fig. 2(h) will rotate clockwise by π/2, and will become Fig. 2(i). Hence, by combining the signal outputs from MZM_1 and MZM_2, we can observe a single sideband signal with suppressed carrier (at ω_0-ω_{RF}), as shown in Fig. 2(j). Although frequency component at ω_0 + $3\omega_{RF}$ also appears, however its magnitude is small and can be neglected.

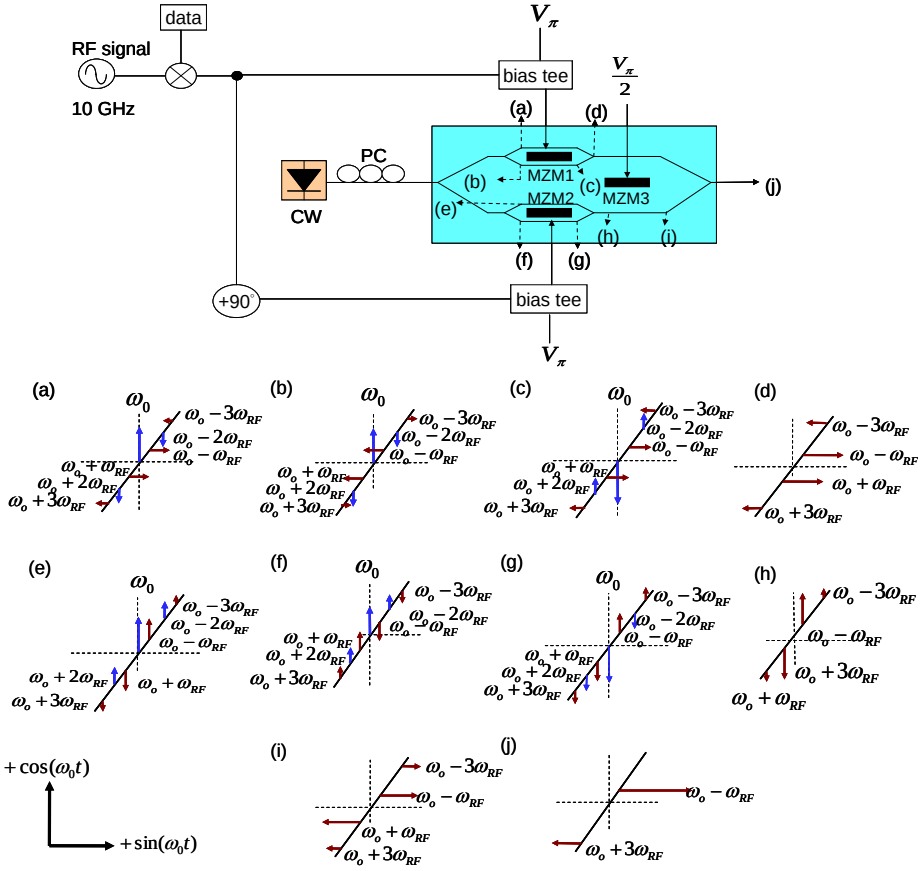

Fig. 2. Schematic of the architecture of the ONU using a DP-MZM. Insets: schematic optical spectra at the corresponding point in the DP-MZM.

4. Network experiment

Figure 3 shows the proposed architecture of the DWDM LR-PON. A wavelength allocation plan consists of 40 channels at 100 GHz channel spacing are included. One advantage of this architecture is that all the optoelectronic components are placed in a controlled environments (inside the remote node (RN) and the CO), where electrical power supply is already present. For the upstream signal, in the RN a CW carrier at 1548 nm was launched to a 3-dB fiber

#140988 - $15.00 USD Received 12 Jan 2011; revised 7 Feb 2011; accepted 7 Feb 2011; published 1 Mar 2011

coupler, a variable optical attenuator (VOA), which was used to emulate the PON split-ratio, and a 25 km drop single-mode fiber (SMF), before entering the ONU. In the colorless ONU, a loop-back configuration was achieved by an optical circulator (OC). The distributed CW carrier was first amplified by a semiconductor optical amplifier (SOA) (Gain = 20 dB, noise figure = 8 dB) and then coupled into the DP-MZM. It was electrically driven by a 10 GHz RF up-converted 2.5 Gb/s NRZ signal at pseudo-random binary sequence (PRBS) 2^{31}-1 in-phase and quadrature-phase respectively as described in section 3. Semiconductor based modulator could be more practical in real network implementation [11]. Another SOA with similar characteristics was used at the DP-MZM output to compensate the modulator loss. The output power at the ONU was about 5 dBm. The upstream signal was then sent back to the CO through the same drop fiber, a red/blue (R/B) filter, an EDFA (Gain = 27 dB, noise figure = 5 dB) and an arrayed waveguide grating (AWG) (Gaussian shaped, 3-dB width of 50 GHz) at the RN. Then the upstream signal was sent back to the receiver (Rx) at CO via 75 km SMF feeder fiber. An optical pre-amplified Rx at the CO was used. It consisted of an EDFA (Gain = 21 dB, noise figure = 5 dB), a tunable bandpass filter (TBF) (3-dB width of 50 GHz) and a PIN photodiode (bandwidth of 3 GHz). No dispersion compensation was used in the experiment. Inset of Fig. 3 shows the measured optical spectra (resolution of 0.01 nm) of the distributed CW carrier and the NRZ upstream signal after wavelength-transition. The suppression ratio of the upstream signal and the center wavelength are > 18 dB. The RB tolerance can be significantly improved by the reduction in the spectral overlap.

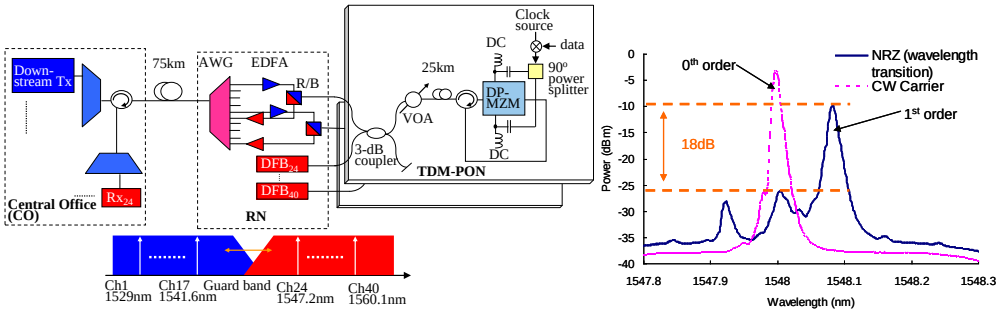

Fig. 3. Architecture of the DWDM LR-PON. R/B: red/blue filter, RN: remote node, VOA: variable optical attenuator. Inset: measured optical spectrum of the upstream NRZ signal.

Figures 4(a) and (b) show the bit-error rate (BER) performance of the upstream NRZ signal with wavelength-transition and the conventional NRZ in the LR-PON respectively. We measured ~5 dB power penalty in the wavelength-transition signal when the split-ratio was 512 (VOA set at >-26 together with the 3-dB fiber coupler prior the VOA), without an error-floor. In Fig. 4(b), the conventional NRZ was not able to achieve 64-split and an error-floor appeared at BER of 10^{-7}. BER cannot be measured at split-ratio of 512 at the conventional NRZ case due to the nearly complete eye-closure (inset of Fig. 4(b)). Figure 4(c) shows the BER of the downstream 10 Gb/s (up to 512 splits) NRZ signal, with the eye-diagram after 100 km SMF.

#140988 - $15.00 USD Received 12 Jan 2011; revised 7 Feb 2011; accepted 7 Feb 2011; published 1 Mar 2011

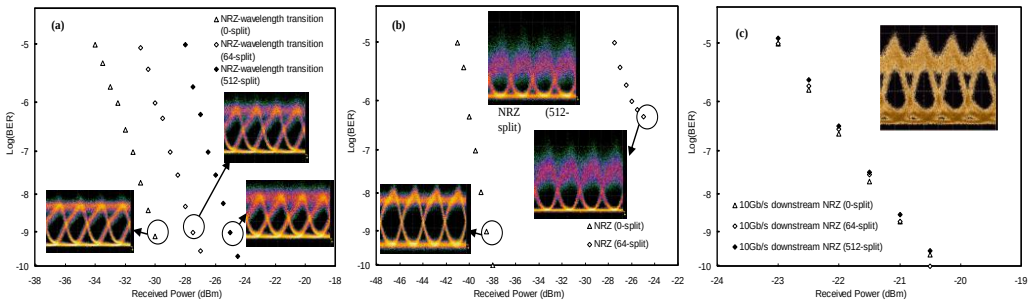

Fig. 4. BER performances of the 2.5 Gb/s upstream signals (a) with wavelength transition and (b) without wavelength transition, and the downstream 10 Gb/s NRZ at different split-ratios in the LR-PON. Insets: corresponding eye diagrams.

5. Conclusion

By using the upstream signal wavelength-transition generated by a commercially available DP-MZM based colorless ONU, both kinds of RB noise sources can be effectively mitigated. A reach extension from typical 20 km PON to 100 km LR-PON with split-ratio increases from 64 to 512 is achieved in the proposed network architecture.

Acknowledgements

This work was supported by the National Science Council, Taiwan, R.O.C., under Contracts NSC 99-2622-E-009-013-CC2, 98-2221-E-009-017-MY3, and 97-2221-E-009-038-MY3.

#140988 - $15.00 USD Received 12 Jan 2011; revised 7 Feb 2011; accepted 7 Feb 2011; published 1 Mar 2011